# Supporting Information

# Control of Photoluminescence Quantum Yield and Long-lived Triplet Emission Lifetime in Organic Alloys

*Zhen Xu,‡ Duane Hean,‡ Jennifer Yuan, and Michael O. Wolf**

Department of C1hemistry, 2036 Main Mall, University of British Columbia, Vancouver, BC, V6T 1Z1, Canada

## General

Solvents were reagent grade and used without any further purification. HPLC grade solvents were used for analyses. 9-H carbazole was purchased from Sigma-Aldrich (China) and purity was confirmed by HPLC. Other purchased chemicals were used without further purification. **CBZ-Br** and **CBZ-Me** were synthesized according to the literature procedure.[1] Afterglow photos were taken using Nikon D750 equipped with Sigma 35 mm F1.4 DG HSM lens (F:1.4, Exposure time: 0.1 s and ISO: 1600). HPLC was performed using an Agilent Technologies 1260 Infinity and an Agilent ZORBAX Extend-C18 column with 4.6 × 150 mm dimensions. The isocratic mobile phase was composed of 25 % acetonitrile, 75 % water with a flow rate of 3 mL/min. The detector wavelength was set to 292 and 360 nm. Electrochemical experiments were performed using a Pine AFCBP1 bipotentiostat in an airtight three-electrode cell with a glassy carbon working electrode, platinum mesh counter electrode, and silver wire pseudo-reference electrode. Cyclic voltammetry (CV) was performed in an electrolyte solution consisting of 0.1 M (n-$Bu_4N$)$PF_6$ (recrystallized 4 times from EtOH) in anhydrous $CH_2Cl_2$ sparged with $N_2$ prior to use. CV experiments were executed with sweep rates of 100 mV $s^{-1}$. Potentials were recorded vs. ferrocene as an added internal standard.

## X-Ray Diffraction

Single crystal X-ray data were collected using a Bruker APEX DUO diffractometer with graphite monochromated Mo Kα radiation (λ = 0.71073 Å) at 100 K. Raw frame data were processed using APEX2.[2] The program SAINT+, v. 7.683 was used to reduce the data and the program SADABS[3] was used to make corrections to the empirical absorptions. Space group assignments were made using XPREP[4] on all compounds. In all cases, the structures were solved in the Olex2[5] suite of programs using Intrinsic Phasing[6] and refined using full-matrix least-squares/difference Fourier techniques on $F^2$ using SHELXL.[6] All non-hydrogen atoms were refined anisotropically. Diagrams and publication material were generated using CrystalMaker.

## POM Microscopy

Microscopy images were collected on an Olympus BX53M polarizing microscope with an Olympus UC90 camera equipped with a λ = 530 nm filter.

**Spectroscopy**

$^{1}$H NMR experiments were collected using a Bruker AV-400 spectrometer and referenced first to TMS and then to the residual protonated solvent peak. NMR solvents (Sigma Aldrich) were used as received. Steady-state and time-resolved photoluminescence spectra were collected using a Photon Technology International (PTI) QuantaMaster 400 fluorimeter utilizing a 75 W Xe arc lamp and a Horiba 359 nm Spectral LED as the sources, respectively. Fluorescence lifetime data were collected using QuantaMaster 400 with a 375 nm pulsed laser. Phosphorescence lifetime data were collected using Horiba Yvon Fluorocube with a 359 nm Horiba spectral LED with band-pass and long-pass filters. The photoluminescence lifetime data were fitted using the DAS6 Data Analysis software package. Samples for low-temperature spectroscopy and lifetime measurements were cooled using an Oxford Instruments Optistat DN.

**Quantum yields**

Quantum yields (QY) were measured using an Edinburgh Instruments barium sulfate coated integrating sphere (diameter, SC-30 sample module) fitted on a FS5 spectrofluorometer. Single crystal samples were placed in the middle of a 10 mm diameter PTFE sample holder (tray), enclosed by a quartz cap (Figure S1). The typical size of crystals was approximately 0.5 × 0.5 × 0.5 mm. The excitation wavelength was set to 380 nm. The sample was excited by direct illumination. The settings were set for maximization of the emission signal before saturating the detector with excitation light (excitation bandwidth = 12 nm, emission bandwidth 0.55-0.60 nm). The reference sample was measured with just the tray and cap (no single crystal). Each sample was run in triplicate, with each quantum yield measurement coming from a new crystal (if available). Measurements proved repeatable and errors are given as standard deviations.

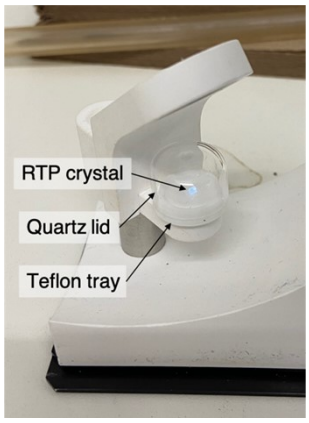


**Figure S1.** Pull-out drawer for Edinburgh Instruments SC-30 sample module with solid sample holder (PTFE tray) and quartz cap. The crystal is under 365 nm excitation under ambient lighting.

**Crystallography**

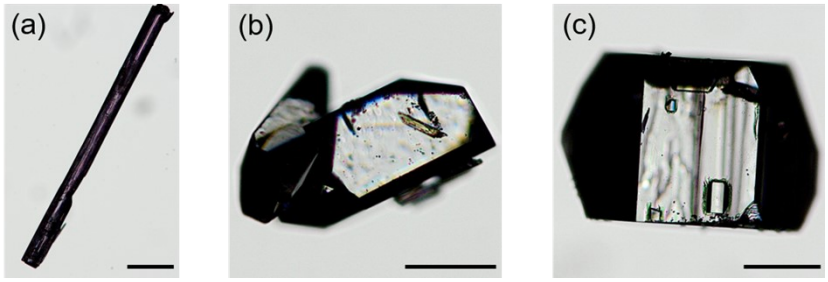


**Figure S2.** Typical crystal morphology of (a) **CBZ-Br** (RTP) (b) **CBZ-Br** (TADF) and (c) **CBZ-Me**. Scale bars are 200 µm.

**Table S1**. Literature unit cell parameters of **CBZ-Br** (RTP), **CBZ-Br** (TADF) and **CBZ-Me**.

| | **CBZ-Br (RTP)** | **CBZ-Br (TADF)** | **CBZ-Me** |
|---|---|---|---|
| CCDC No. | 2016853 | 1533213 | 1503835 |
| a (Å) | 19.509(4) | 11.5066(15) | 11.6578(3) |
| b (Å) | 5.1417(10) | 10.2017(13) | 10.0346(3) |
| c (Å) | 15.023(3) | 12.349(16) | 12.3140(4) |
| α (°) | 90 | 90 | 90 |
| β (°) | 103.54(3) | 95.332(4) | 94.619(3) |
| γ (°) | 90 | 90 | 90 |
| Volume (Å$^3$) | 1465.07 | 1443.42 | 1435.83 |
| Space group | P21/c | P21/n | P21/n |

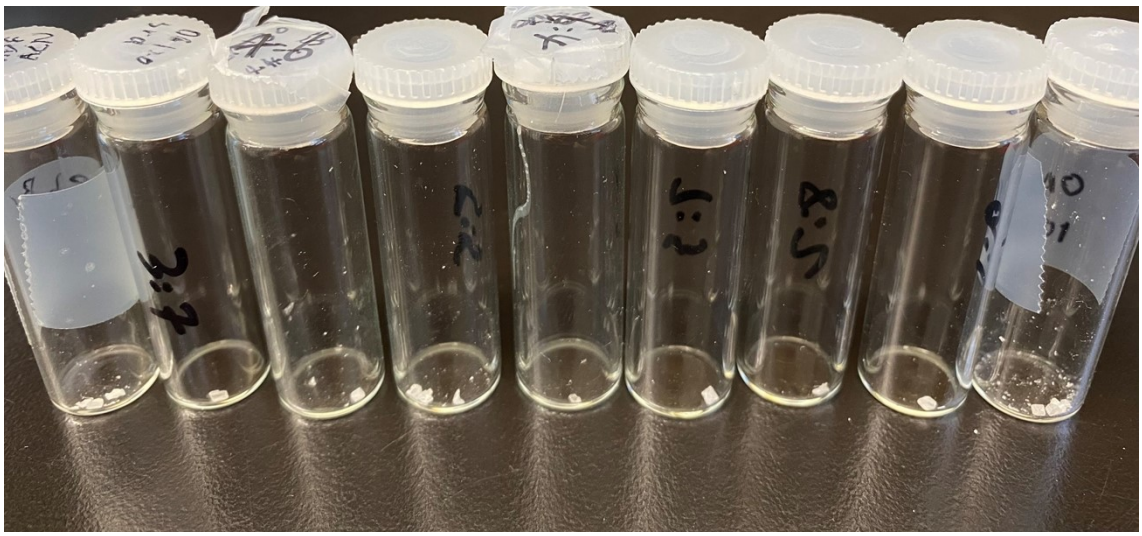

**Figure S3.** Molecular crystals of **CBZ-Br** and organic alloy $\mathbf{Me_xBr_{10-x}}$ where x = 3 to 10, grown from slow evaporation of acetonitrile crystallization experiments

**Table S2**: Unit cell parameters for organic alloy $\mathbf{Me_xBr_{10-x}}$ where x = 3 to 10.

| | $\mathbf{Me_3Br_7}$ | $\mathbf{Me_4Br_6}$ | $\mathbf{Me_5Br_5}$ | $\mathbf{Me_6Br_4}$ | $\mathbf{Me_7Br_3}$ | $\mathbf{Me_8Br_2}$ | $\mathbf{Me_9Br_1}$ |
|---|---|---|---|---|---|---|---|
| a (Å) | 11.5265(6) | 11.5680(7) | 11.5657(6) | 11.5850(7) | 11.5964 (10) | 11.6030(8) | 11.6141(6) |
| b (Å) | 10.1543(5) | 10.1429(5) | 10.1316(5) | 10.1100(6) | 10.0911(8) | 10.0711(6) | 10.0515(5) |
| c (Å) | 12.3229(7) | 12.3305(7) | 12.3187(6) | 12.3005(7) | 12.3080(1) | 12.3038(8) | 12.2961(6) |
| β (°) | 95.063(2) | 95.097(3) | 95.031(2) | 94.882(4) | 94.854(2) | 94.846(2) | 94.745(1) |
| Volume (Å$^3$) | 1436.69(13) | 1441.05 (14) | 1437.92(12) | 1435.46(4) | 1435.1(2) | 1432.62(16) | 1430.52(12) |

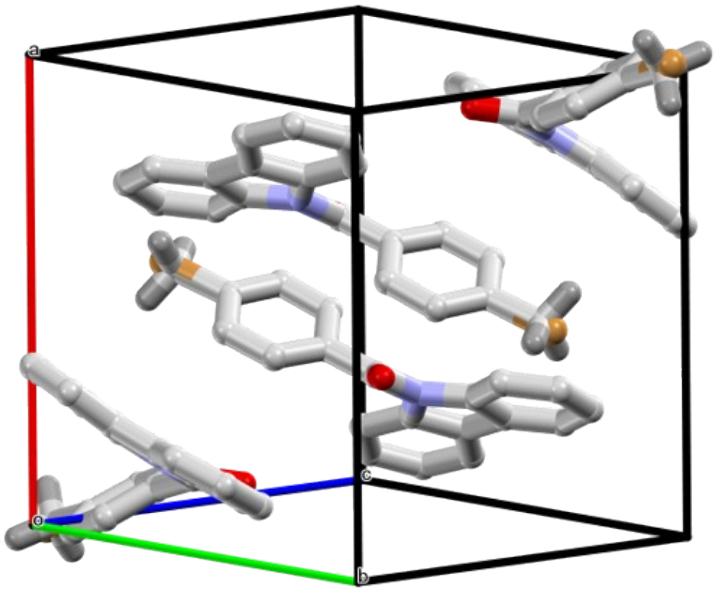

**Figure S4.** Representative superposition of the binary assemblies for organic alloy **$Me_5Br_5$** in the unit cell. C light gray, H dark gray, N blue, O red, Br brown. Aromatic hydrogens are excluded for clarity.

**Table S3.** Mole ratio and site occupancy factors for organic alloy **$Me_xBr_{10-x}$** where x = 3 to 10, and the corresponding photophysical parameters.

| | ***CBZ-Me*: *CBZ-Br* Ratio** | | | ***Lifetime*** | | | | |
|---|---|---|---|---|---|---|---|---|
| | Mole Ratio | Site Occupancy Factor | $^1$H NMR Integration Ratio | Ambient Conditions | | Long lived under He (ms) | Long lived at 77 K (ms) | ***PLQY (%)*** |
| | | | | Long lived (ms) (Chi-squared) | Fluorescence (ns) | | | |
| ***$Me_3Br_7$*** | 30:70 | 35.91(15) : 64.09(15) | 29.35 : 70.65 | 107 (1.00) | 1.38 | 133 | 29.3 (0.03), 271 (0.421), 558 (0.549) | 14.0 |
| ***$Me_4Br_6$*** | 40:60 | 43.99(12) :56.01(12) | 40.1 : 59.9 | 119 (0.89) | 1.38 | 135 | 291. (0.036), 302 (0.479), 570 (0.585) | 10.2 |
| ***$Me_5Br_5$*** | 50:50 | 52.76(12) : 47.24(12) | 50.9 : 49.1 | 126 (0.93) | 1.26 | 142 | 37.1 (0.01), 353 (0.431), 621 (0.559) | 19.7 |

| | | | | | | | | |
|---|---|---|---|---|---|---|---|---|
| ***Me$_6$Br$_4$*** | 60:40 | 55.70(2) : 44.30(2) | 61.35 : 38.65 | 134 (0.83) | 1.25 | 167 | 36.6 (0.012) 370 (0.4), 657 (0.588) | 10.8 |
| ***Me$_7$Br$_3$*** | 70:30 | 71.32(11) : 28.68(11) | 72.2 : 27.8 | 140 (1.02) | 1.19 | 171 | 44.2 (0.01), 387 (0.349), 693 (0.641) | 26.9 |
| ***Me$_8$Br$_2$*** | 80:20 | 81.25(9) : 18.75(9) | 75.95 : 24.05 | 170 (1.07) | 1.02 | 178 | 670 | 24.1 |
| ***Me$_9$Br$_1$*** | 90:10 | 91.21(8) : 8.790(8) | 89.85 : 10.15 | 197 (1.05) | 0.9 | 205 | 548 (0.456), 785 (0.544) | 26.7 |

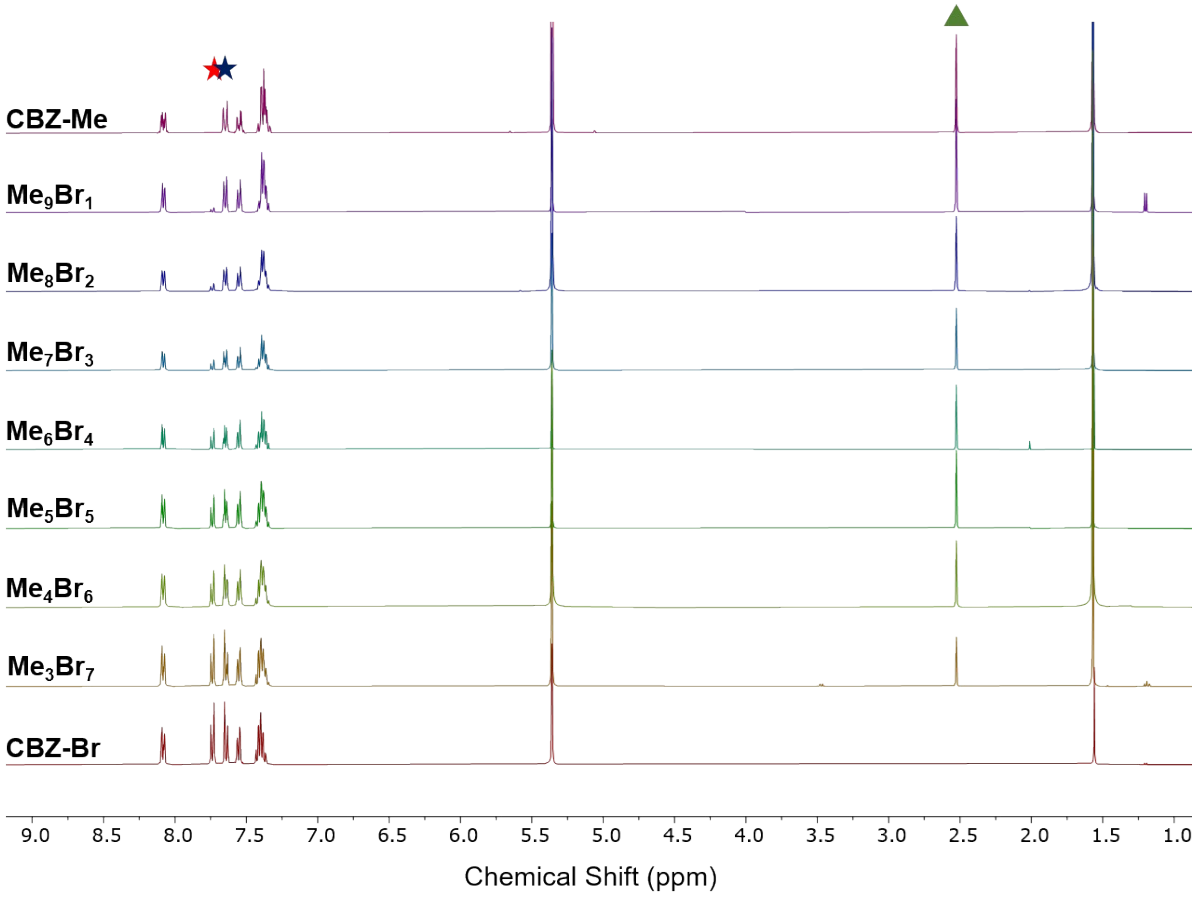


**Figure S5.** $^1$H NMR (400 MHz) spectra of **CBZ-Me**, **CBZ-Br** and the organic alloys **Me$_x$Br$_{10-x}$** where x = 3 to 10, in $CD_2Cl_2$. Peaks marked with stars and triangles were used in integration analysis to determine the ratio of **CBZ-Me** : **CBZ-Br** in each organic alloy crystal sample. Peaks at 5.3 ppm and 1.5 ppm correspond to residual solvent and water respectively. Peaks between 1.0 ppm and 2.0 ppm are impurity peaks resulting from paratone oil used to mount

crystals on a loop for x-ray diffraction.

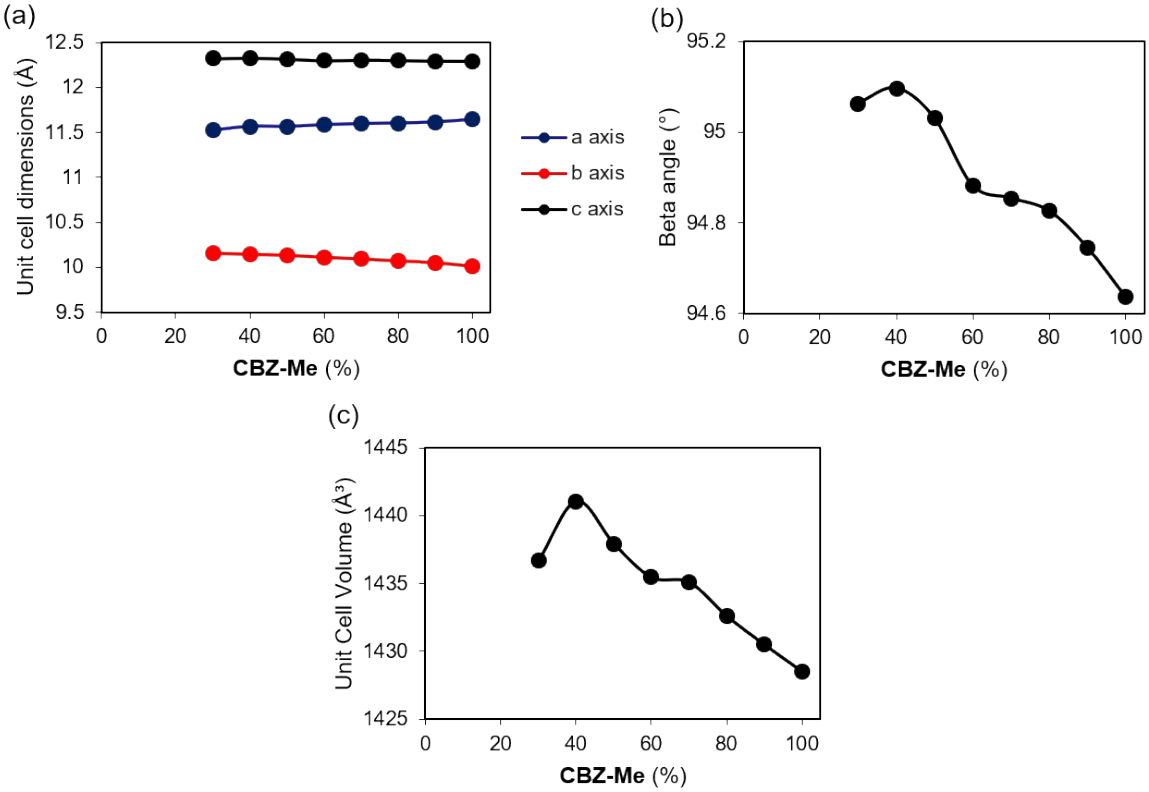


**Figure S6.** (a) Unit cell dimension variation with increasing **CBZ-Me** composition. (b) Decreasing β angle with increasing **CBZ-Me** composition (c) Decreasing unit cell volume with increasing **CBZ-Me** composition.

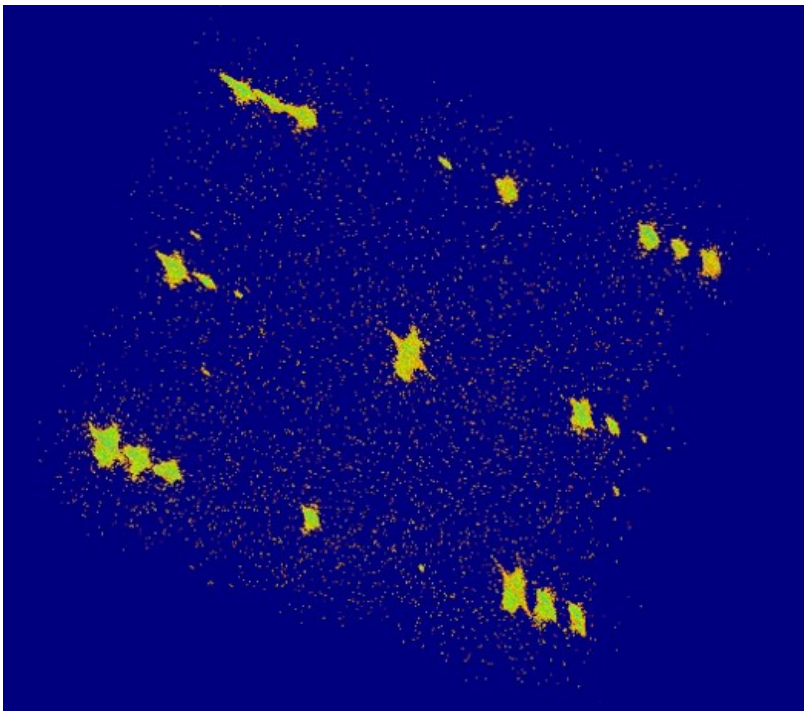

**Figure S7.** Representative diffraction pattern of **$Me_5Br_5$** showing Bragg peaks and noise from the detector as view in MAX3D (Britten/Guan). The absence of diffuse scattering peaks or streaks indicates that the amount of short range order in the disordered regions is very low.

## Photophysics of Parent Compounds

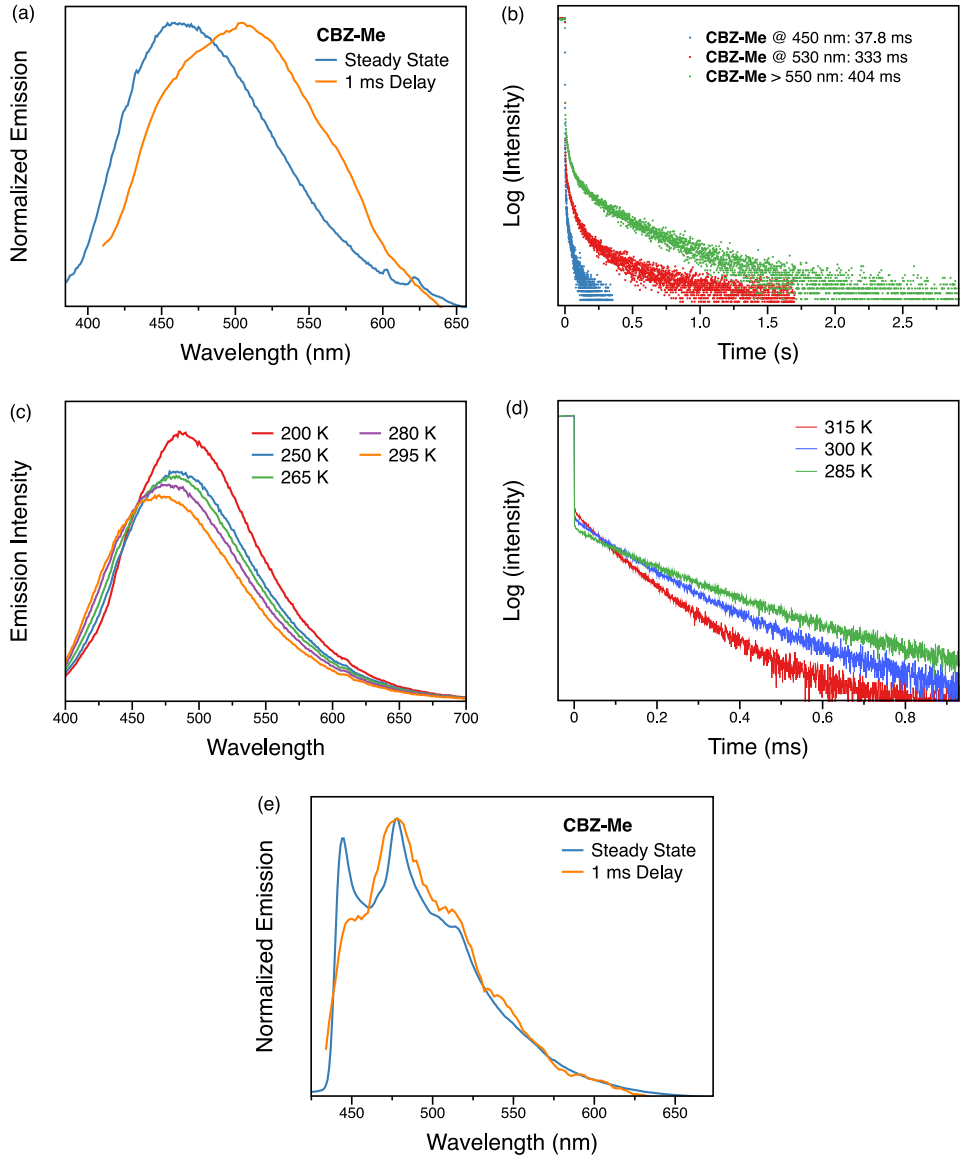


**Figure S8**. Steady state (blue line) and 1 ms delay (orange line) photoluminescence spectrum of **CBZ-Me** (a) under air at room temperature and (e) under Helium at 77 K. (b) Phosphorescence decay of **CBZ-Me** measured under air at room temperature at 450 nm, 530 nm and above 550 nm. Variable-temperature (c) steady state photoluminescence spectrum and (d) phosphorescence decay of **CBZ-Me** under helium atmosphere.

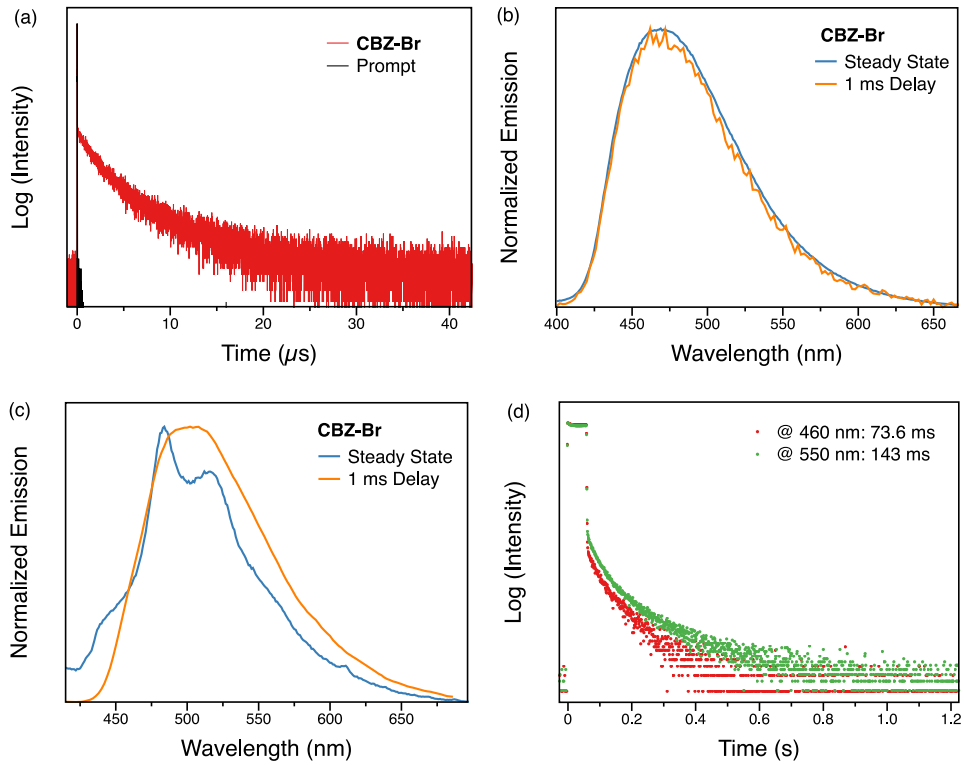


**Figure S9**. (a) Microsecond photoluminescence decay of **CBZ-Br** under air at room temperature. Steady state (blue line) and 1 ms delay (orange line) photoluminescence spectrum of **CBZ-Br** (b) under air at room temperature and (c) under helium at 77 K. (d) Millisecond photoluminescence decay of **CBZ-Br** above 500 nm under air at room temperature

## Photophysics of Organic Alloys

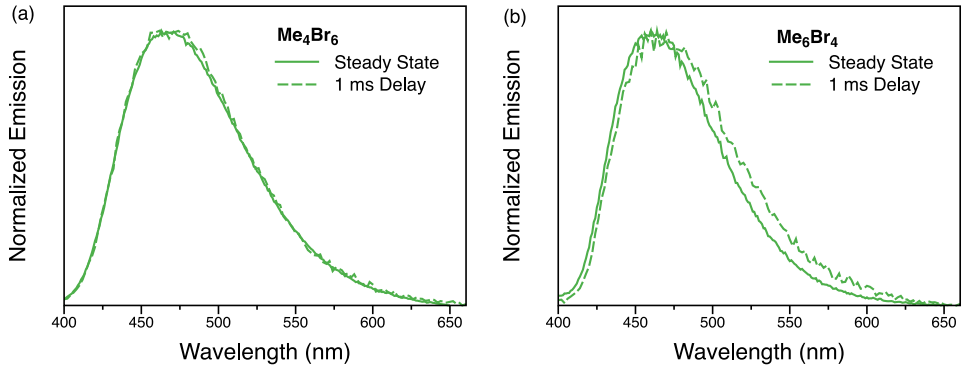

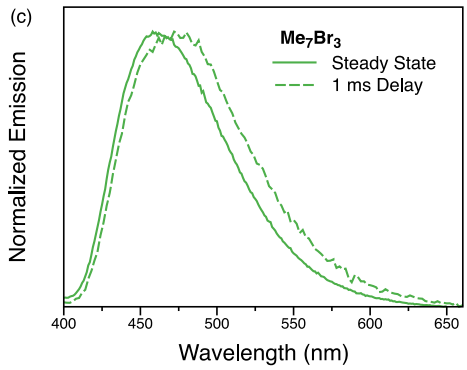


**Figure S10**. Steady state (solid line) and 1 ms delay (dashed line) photoluminescence spectrum of (a) **$Me_4Br_6$**, (b) **$Me_6Br_4$** and (c) **$Me_7Br_3$** under air at room temperature.

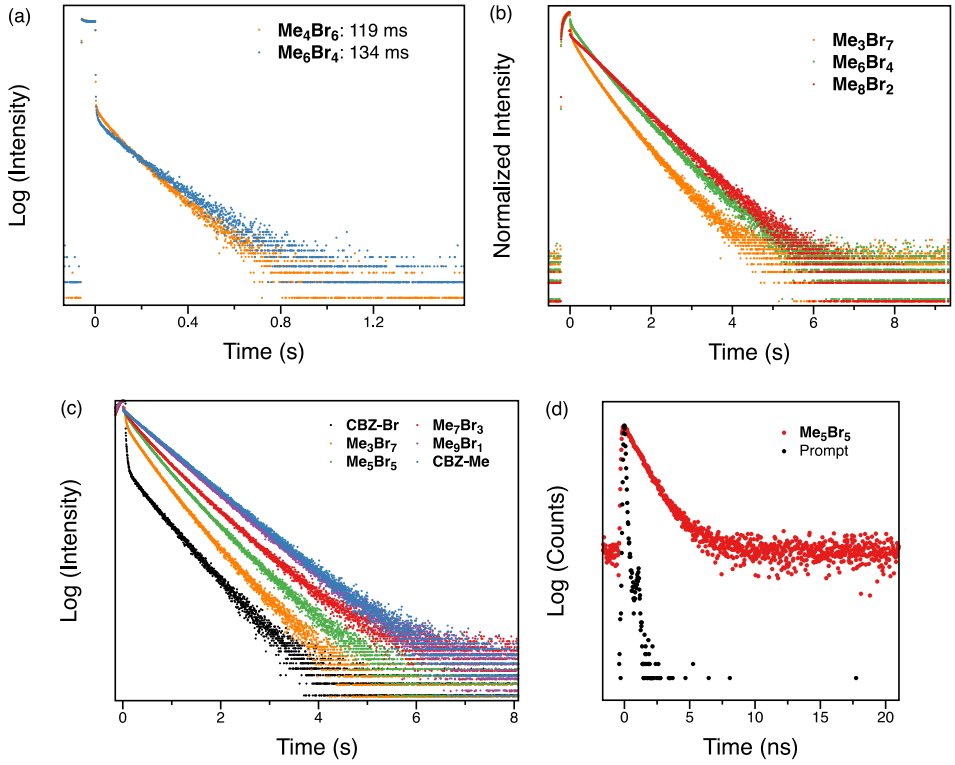


**Figure S11**. Phosphorescence decay of (a) **$Me_4Br_6$** and **$Me_6Br_4$** under air at room temperature and (b) **$Me_4Br_6$**, **$Me_6Br_4$** and **$Me_8Br_2$** at 77 K. (c) Phosphorescence decay of **CBZ-Br**, **$Me_3Br_7$**, **$Me_5Br_5$**, **$Me_9Br_1$** and **CBZ-Me** at 77 K. (d) fluorescence decay of **$Me_5Br_5$** under air at room temperature.

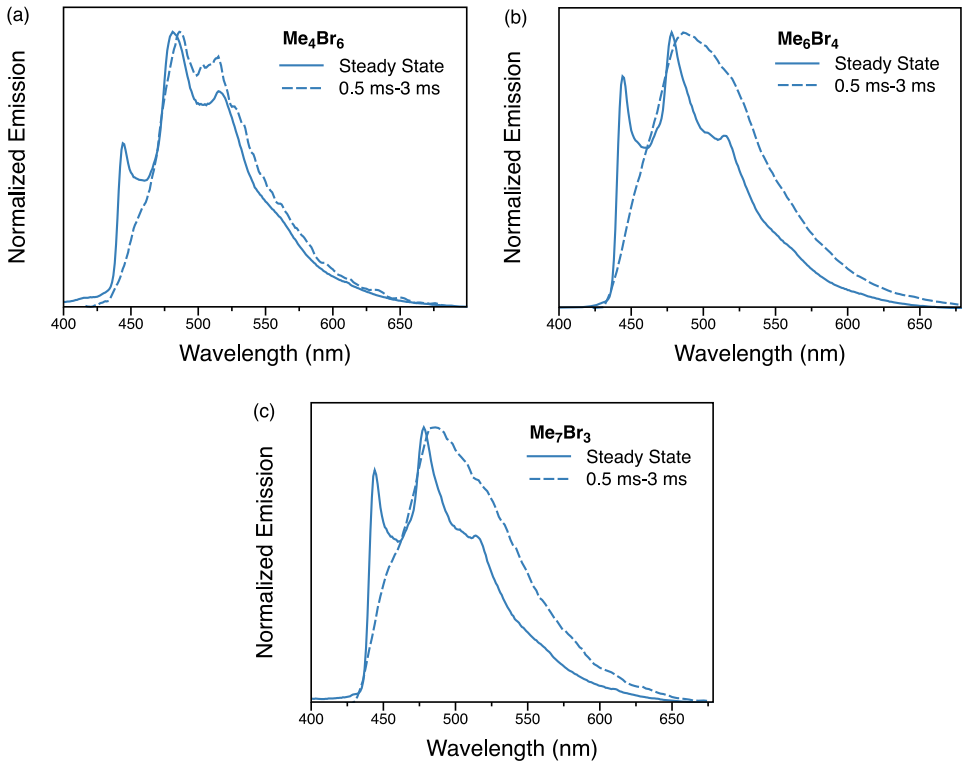


**Figure S12**. Steady state (solid line) and 1 ms delay (dashed line) photoluminescence spectra of (a) $\mathbf{Me_4Br_6}$, (b) $\mathbf{Me_6Br_4}$ and (c) $\mathbf{Me_7Br_3}$ under air at 77 K.

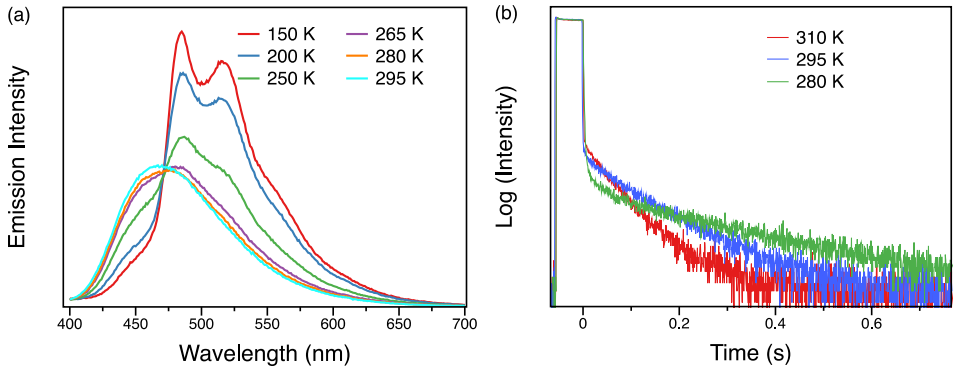


**Figure S13.** Variable-temperature (a) steady state photoluminescence spectra and (b) phosphorescence decay of $\mathbf{Me_3Br_7}$ under helium atmosphere.

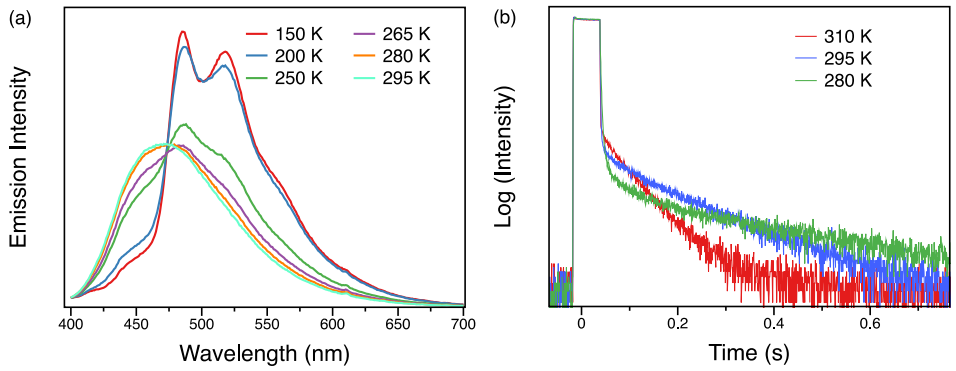


**Figure S14.** Variable-temperature (a) steady state photoluminescence spectra and (b) phosphorescence decay of **$Me_4Br_6$** under helium atmosphere.

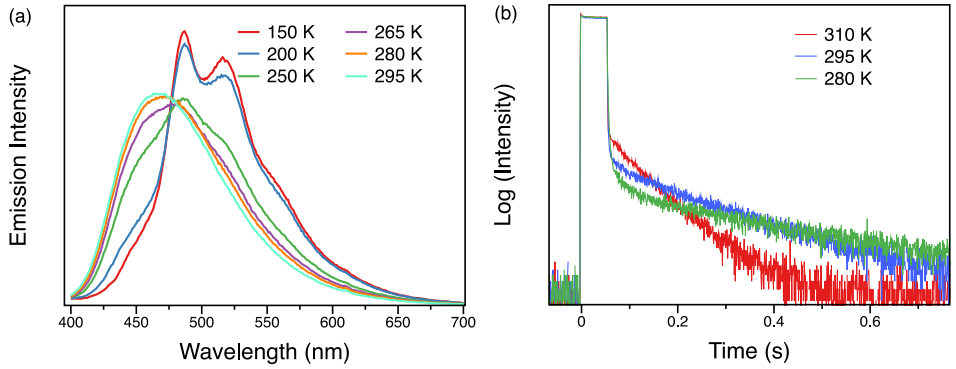


**Figure S15.** Variable-temperature (a) steady state photoluminescence spectra and (b) phosphorescence decay of **$Me_6Br_4$** under helium atmosphere.

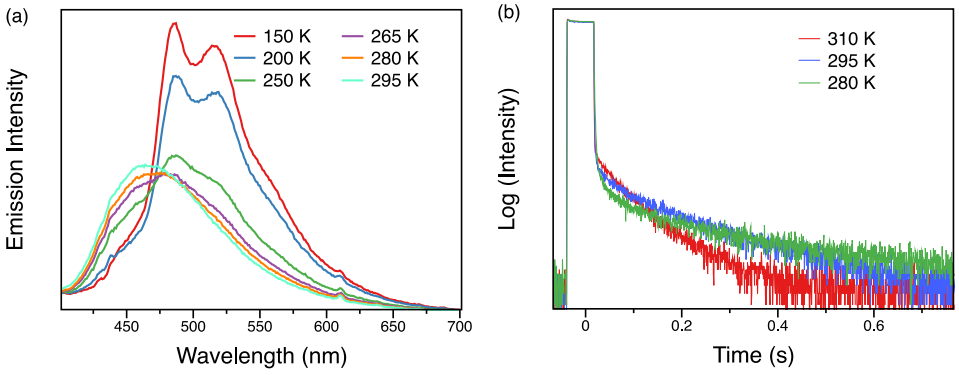


**Figure S16.** Variable-temperature (a) steady state photoluminescence spectra and (b) phosphorescence decay of **$Me_7Br_3$** under helium atmosphere.

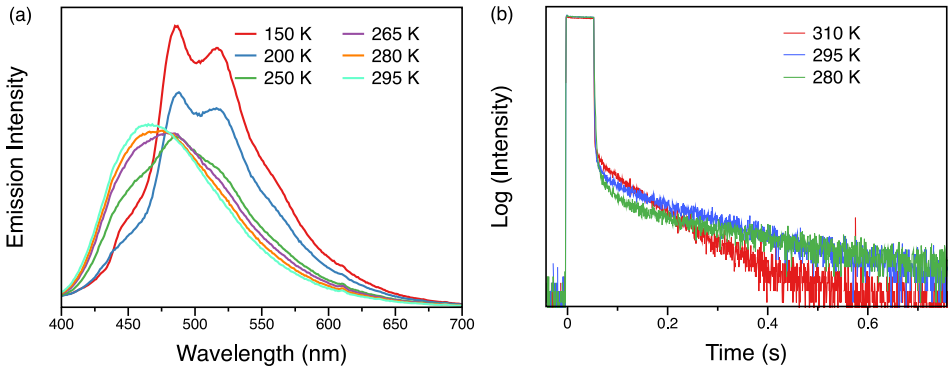


**Figure S17.** Variable-temperature (a) steady state photoluminescence spectra and (b) phosphorescence decay of **$Me_8Br_2$** under helium atmosphere.

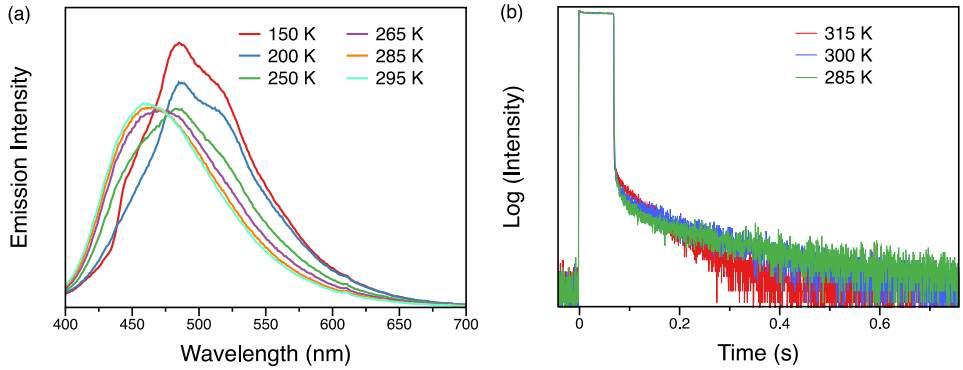


**Figure S18.** Variable-temperature (a) steady state photoluminescence spectra and (b) phosphorescence decay of **$Me_9Br_1$** under helium atmosphere.

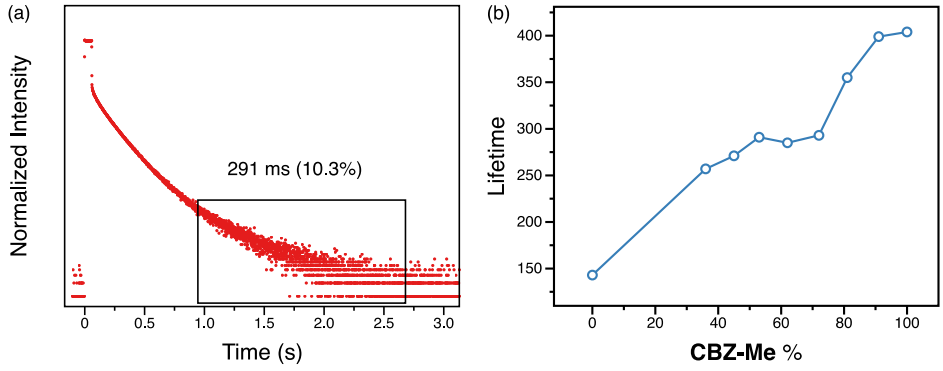


**Figure S19.** (a) Phosphorescence decay of **$Me_5Br_5$** at 550 nm under air at room temperature. (b) Plots of longest decay lifetimes at 550 nm under air at room temperature against **CBZ-Me** ratios.

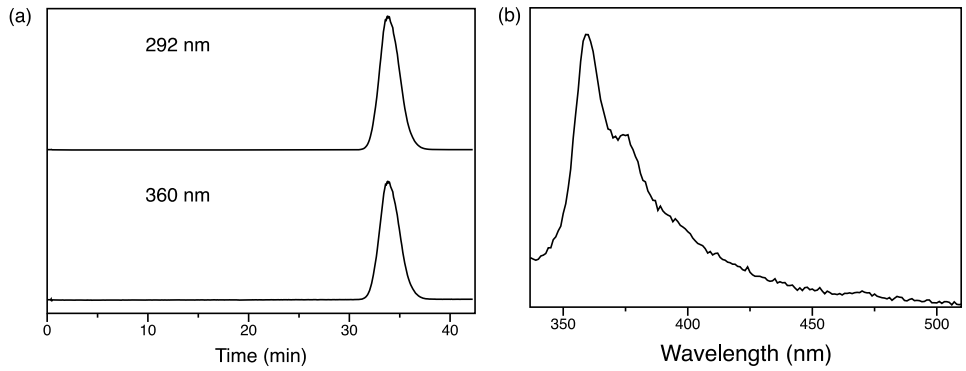


**Figure S20.** (a) HPLC trace of recrystallized 9-H carbazole starting materials monitored at 292 and 360 nm. (b) Fluorescence spectrum of carbazole crystals.

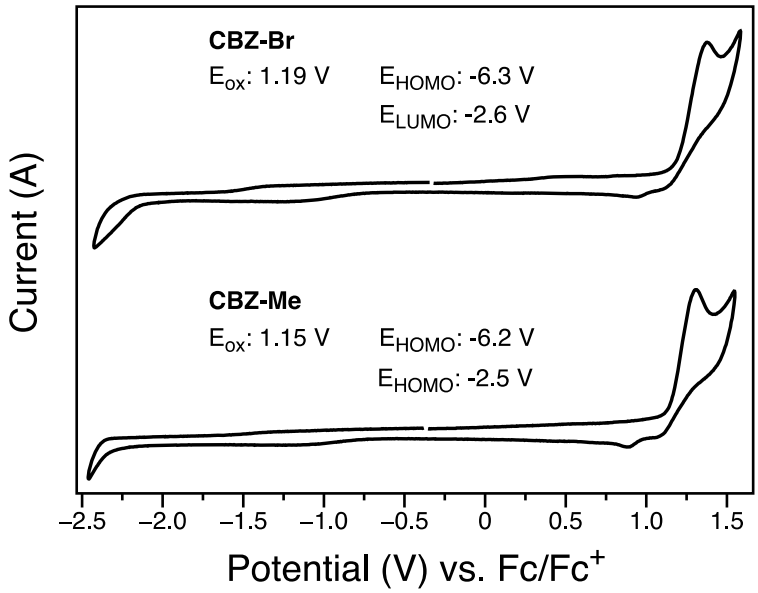


**Figure S21.** Cyclic voltammetry of **CBZ-Br** and **CBZ-Me** in $CH_2Cl_2$ at $1 \times 10^{-3}$ M. The numbers were onset values by tangents.

**Table S4.** Crystal data for organic alloy $\mathbf{Me_xBr_{10-x}}$ where x = 3 to 10.

| **Compound** | $\mathbf{Me_3Br_7}$ | $\mathbf{Me_4Br_6}$ | $\mathbf{Me_5Br_5}$ | $\mathbf{Me_6Br_4}$ | $\mathbf{Me_7Br_3}$ | $\mathbf{Me_8Br_2}$ | $\mathbf{Me_9Br_1}$ |
|---|---|---|---|---|---|---|---|
| **Empirical formula** | $C_{19.36}H_{13.07}Br_{0.64}$ NO | $C_{19.44}H_{13.32}Br_{0.56}$ NO | $C_{19.47}H_{13.41}Br_{0.53}$ NO | $C_{19.56}H_{13.67}Br_{0.44}$ NO | $C_{19.71}H_{14.14}Br_{0.29}$ NO | $C_{19.81}H_{14.44}Br_{0.19}$ NO | $C_{19.91}H_{14.74}Br_{0.09}$ NO |
| **Formula weight** | 327.01 | 321.66 | 319.55 | 314.04 | 303.98 | 297.49 | 291.01 |
| **Temperature/K** | 100 | 120.0 | 100 | 100.0 | 100.0 | 100.15 | 100 |
| **Crystal system** | monoclinic | monoclinic | monoclinic | monoclinic | monoclinic | monoclinic | monoclinic |
| **Space group** | $P2_1/n$ | $P2_1/n$ | $P2_1/n$ | $P2_1/n$ | $P2_1/n$ | $P2_1/n$ | $P2_1/n$ |
| **a/Å** | 11.5265(6) | 11.5680(7) | 11.5657(6) | 11.5850(7) | 11.5964(10) | 11.6030(8) | 11.6141(6) |
| **b/Å** | 10.1543(5) | 10.1429(5) | 10.1316(5) | 10.1100(6) | 10.0911(8) | 10.0711(6) | 10.0515(5) |
| **c/Å** | 12.3229(7) | 12.3305(7) | 12.3187(6) | 12.3005(7) | 12.3080(1) | 12.3038(8) | 12.2961(6) |
| **α/°** | 90 | 90 | 90 | 90 | 90 | 90 | 90 |
| **β/°** | 95.063(2) | 95.097(2) | 95.031(2) | 94.882(4) | 94.854(2) | 94.846(2) | 94.7450(10) |
| **γ/°** | 90 | 90 | 90 | 90 | 90 | 90 | 90 |

| | | | | | | | |
|---|---|---|---|---|---|---|---|
| **Volume/Å$^3$** | 1436.69(13) | 1441.05(14) | 1437.93(12) | 1435.46(15) | 1435.1(2) | 1432.62(16) | 1430.52(12) |
| **Z** | 4 | 4 | 4 | 4 | 4 | 4 | 4 |
| **$\rho_{calc}$g/cm$^3$** | 1.512 | 1.483 | 1.476 | 1.453 | 1.407 | 1.379 | 1.351 |
| **μ/mm$^{-1}$** | 1.868 | 1.633 | 1.546 | 1.313 | 0.881 | 0.604 | 0.326 |
| **F(000)** | 667.0 | 658.0 | 655.0 | 646.0 | 630.0 | 620.0 | 609.0 |
| **Crystal size/mm$^3$** | 0.399 × 0.389 × 0.379 | 0.381 × 0.38 × 0.379 | 0.398 × 0.378 × 0.222 | 0.399 × 0.345 × 0.322 | 0.389 × 0.365 × 0.312 | 0.387 × 0.345 × 0.312 | 0.399 × 0.389 × 0.378 |
| **Radiation** | MoKα (λ = 0.71073) | MoKα (λ = 0.71073) | MoKα (λ = 0.71073) | MoKα (λ = 0.71073) | MoKα (λ = 0.71073) | MoKα (λ = 0.71073) | MoKα (λ = 0.71073) |
| **2Θ range for data collection/°** | 4.638 to 61.126 | 4.628 to 61.08 | 4.632 to 61.112 | 4.638 to 61.402 | 4.634 to 61.074 | 4.634 to 61.134 | 4.636 to 61.232 |
| **Index ranges** | -16 ≤ h ≤ 16, -9 ≤ k ≤ 14, -17 ≤ l ≤ 17 | -16 ≤ h ≤ 16, -14 ≤ k ≤ 11, -17 ≤ l ≤ 17 | -16 ≤ h ≤ 16, -14 ≤ k ≤ 13, -17 ≤ l ≤ 17 | -16 ≤ h ≤ 15, -14 ≤ k ≤ 14, -17 ≤ l ≤ 17 | -16 ≤ h ≤ 16, -14 ≤ k ≤ 9, -17 ≤ l ≤ 17 | -16 ≤ h ≤ 16, -14 ≤ k ≤ 13, -17 ≤ l ≤ 17 | -16 ≤ h ≤ 16, -14 ≤ k ≤ 14, -17 ≤ l ≤ 17 |
| **Reflections collected** | 24000 | 27288 | 25444 | 25359 | 23841 | 25717 | 25534 |
| **Independent** | 4369 [$R_{int}$ = | 4402 [$R_{int}$ = | 4414 [$R_{int}$ = | 4401 [$R_{int}$ = | 4369 [$R_{int}$ = | 4386 [$R_{int}$ = | 4395 [$R_{int}$ = |

| | | | | | | | |
|---|---|---|---|---|---|---|---|
| **reflections** | 0.0369, $R_{sigma}$ = 0.0292] | 0.0225, $R_{sigma}$ = 0.0166] | 0.0266, $R_{sigma}$ = 0.0194] | 0.0981, $R_{sigma}$ = 0.0902] | 0.0234, $R_{sigma}$ = 0.0182] | 0.0336, $R_{sigma}$ = 0.0270] | 0.0198, $R_{sigma}$ = 0.0144] |
| **Data/restraints/parameters** | 4369/354/204 | 4402/351/210 | 4414/0/210 | 4401/351/192 | 4369/351/210 | 4386/0/210 | 4395/0/210 |
| **Goodness-of-fit on $F^2$** | 1.043 | 1.024 | 1.027 | 1.046 | 1.066 | 1.041 | 1.040 |
| **Final R indexes [I>=2σ (I)]** | $R_1$ = 0.0339, $wR_2$ = 0.0775 | $R_1$ = 0.0284, $wR_2$ = 0.0667 | $R_1$ = 0.0300, $wR_2$ = 0.0716 | $R_1$ = 0.0682, $wR_2$ = 0.1966 | $R_1$ = 0.0370, $wR_2$ = 0.0893 | $R_1$ = 0.0367, $wR_2$ = 0.0980 | $R_1$ = 0.0388, $wR_2$ = 0.1028 |
| **Final R indexes [all data]** | $R_1$ = 0.0455, $wR_2$ = 0.0815 | $R_1$ = 0.0355, $wR_2$ = 0.0696 | $R_1$ = 0.0388, $wR_2$ = 0.0752 | $R_1$ = 0.0919, $wR_2$ = 0.2147 | $R_1$ = 0.0458, $wR_2$ = 0.0931 | $R_1$ = 0.0448, $wR_2$ = 0.1020 | $R_1$ = 0.0449, $wR_2$ = 0.1071 |
| **Largest diff. peak/hole / e $Å^{-3}$** | 0.59/-0.41 | 0.38/-0.25 | 0.37/-0.24 | 1.19/-1.15 | 0.38/-0.25 | 0.42/-0.23 | 0.48/-0.23 |

**References**


[1] (a) Y. Xie, Y. Ge, Q. Peng, C. Li, Q. Li, Z. Li, *Adv. Mater.* **2017**, *29*, 1606829; (b) S. Cai, H. Shi, J. Li, L.Gu, Y. Ni, Z. Cheng, S. Wang, W. Xiong, L. Li, Z. An, W. Huang, *Adv. Mater.* **2017**, *29*, 1701244.

[2] APEX2 (Version 2014.11-0), Bruker AXS Inc. Madison, Wisconsin, **2014**.

[3] SADABS (Version 2014/5), Bruker AXS Inc. Madison, Wisconsin, **2014**.

[4] SAINT+ (Version 8.43A), Bruker AXS Inc. Madison, Wisconsin, **2013**.

[5] O. V. Dolomanov, L. J. Bourhis, R. J. Gildea, J. A. K. Howard, H. Puschmann, *J. Appl. Crystallogr.* **2009**, *42*, 339–341.

[6] G. M. Sheldrick, *Acta Crystallogr. Sect. C Struct. Chem.* **2015**, *71*, 3–8.